RSC Advances

ROYAL SOCIETY OF CHEMISTRY

www.rsc.org/advances

Synthesis, characterization and photocatalytic studies of mesoporous silica grafted Ni(II) and Cu(II) complexes

G. Ramanjaneya Reddy,[a] and S. Balasubramanian[a]*

[a]*Department of Inorganic Chemistry, School of Chemical Sciences, University of Madras, Guindy Campus, Chennai-600 025, India. E-mail:bala2010@yahoo.com; Tel: +91 9444016707, 044 22202794, Fax: +91 4422300488.*

Abstract

The mesoporous silica grafted nickel(II) and copper(II) complexes of the Schiff base ligand were synthesized. The functionalization of the ligand was achieved by the Schiff base condensation of 3-APTES and O,O'-mono methylene bis(salicylidene). The Schiff base moiety was subsequently grafted with MCM41, followed by complexation with the metal salts. The compounds were characterized by spectral(Fourier Transform Infrared spectroscopy (FTIR), diffuse reflectance UV–Vis spectroscopy (DRS/UV-Vis), X-ray diffraction (XRD), X-ray Photoelectron Spectroscopy (XPS)), thermal (Thermo Gravimetric Analysis (TGA)) microscopic(High Resolution Transmission Electron Microscopy (HRTEM)) and surface Brunauer–Emmett–Teller (BET) method, N_2-sorption isotherms) analysis**.** The compounds were employed in the photo oxidation of Methyl Orange (MO) and Reactive Red198 (RR). The copper complex exhibits higher activity in the photo degradation of the dyes. The reusable photocatalysts show comparable activity to that of fresh catalyst without loss of their catalytic nature

Introduction

Metal organic frameworks (MOFs) are an emerging class of porous crystalline materials, which can be designed at a molecular level to perform many processes including catalysis.[1] The hybrid materials have good textural properties like high surface area, porosity, uniform crystalline size and thermal stability.[2] Moreover, this class of materials find applications such as gas storage, separation, proton conductance, sensing, drug delivery, magnetism, and heterogeneous catalysis.[3-7] The homogeneous catalysts have been employed in many organic transformations.[8] The transition metal complexes act as homogenous catalysts in organic reactions.[9] However, the recovery and reuse of the catalysts are very challenging tasks in reaction mixture, where as the heterogeneous

catalysts can overcome these disadvantages.[10] The silica based inorganic supports play major role in catalytic reactions and structurally build up with the SiO_4 tetrahedral units with voids and they can act as hosts for the guest molecules. The host-guest interaction plays a major role in the field of photocatalysis. The metal activated silica supports were used as adsorbents. Their porous structures facilitate the diffusion of substrates and products and make them an ideal platform to incorporate catalytic centres.

Non-catalytic methods with stoichiometric, toxic, corrosive and expensive oxidants such as dichromate, permanganate, hydrofluoric acid, sulphuric acid, and peroxy acids under stringent conditions of high pressure and/or temperature have been widely used for dye molecule oxidations.[11] These reactions are often carried out in high concentration and in environmentally unfriendly organic solvents. To achieve decolorization of the xanthene class of dyes, initially the azo bonded moiety should be cleaved catalytically. Aerobic processes utilize oxygen, which can inhibit azo (N=N) bond cleavage.[12] However, enhancement of catalytic activity with nickel(II) and copper(II) based systems are alternative to highly expensive systems such as platinum, diamond, ruthenium, gold and palladium.[13] The mesoporous silica systems grafted with Schiff base moiety can be used as efficient catalysts for degradation of dye molecules such as methyl orange, phenol red, methylene blue, rosebengal, sudan-III and reactive red.[14-18] The development of inexpensive, stable, efficient and band-gap tunable MOF based photocatalysts is still a major challenge, since they have absorbing tendency of the dye molecules by electrostatic interactions with surface containing hydroxyl groups. The high surface area materials have the tendency to absorb and activate the dye molecules to the excited states. The modified mesoporous silica can delocalize the band gap excited electrons of HOMO and LUMO levels of metal complexes. Hence, they minimize the electron-hole recombination besides a relative number of active sites present on the composite surface. Besides, the ability of grafted silica favours photo induced electron-transfer reactions and generate powerful oxidative ion-radical species such as $^{\bullet}OH$, $^{-}O_2$ and $^{+\bullet}O_2H$. This supported system improves the rate of reaction and catalytic activity towards the decolorization of the toxic dyes.[19] There are not many reports on the removal of dyes by silica supported Schiff base Ni(II) and Cu(II) composites and their photocatalytic applications. Hence, the photo degradation of dyes by mesoporous silica supported N_2O_2 tetradentate Schiff base complexes under UV and solar light source has been investigated.

In the present investigation, the mesoporous silica (MCM41) was functionalized with Ni(II) and Cu(II) complexes of N_2O_2 Schiff base ligand by post grafting method. These complexes were used as photocatalysts in the degradation of Methyl orange (MO) and Reactive Red-198 (RR) under UV light irradiation. The activity of the solid supported catalysts was determined by spectrophotometric techniques.

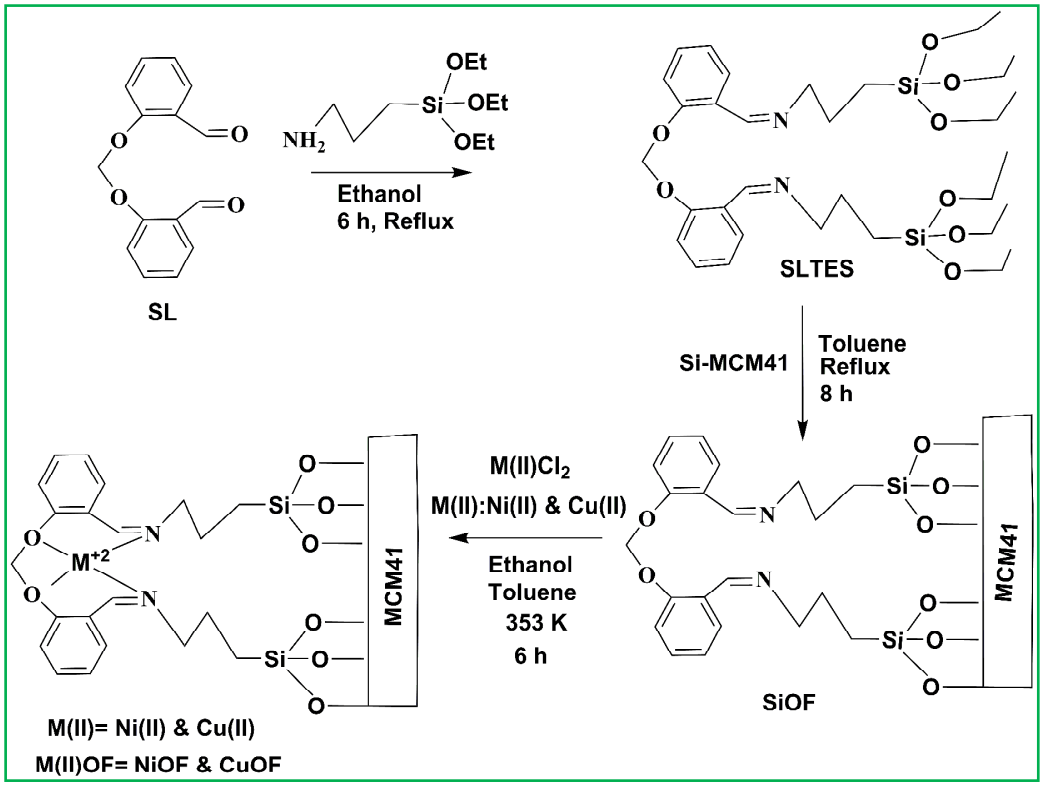

Scheme 1: Grafting of Ni(II) and Cu(II) complexes onto MCM41 by Schiff base condensation of SL and 3-APTES.

Experimental

Materials

Salicylaldehyde, diidomethane (Merck, India), copper chloride, nickel chloride (Qualigens, India), cetyltrimethyl ammonium bromide (CTAB) (LobaChemie. Pvt. Ltd, India), Tetraethoxyorthosilicate (TEOS), 3-APTES (Sigma-Aldrich, India), methyl orange (Merck, India), reactive red-198 (Textile industry, Tamilnadu) and other analar grade chemicals were used without further purification. Millipore water was used throughout the work.

Physicochemical measurements and characterization

The NMR spectra were recorded on a Bruker Avance 400MHz NMR spectrometer. The FTIR spectra were recorded on a FTIR Perkin-Elmer 8300 spectrometer with KBr pellets.The UV-Visible Diffuse Reflectance Spectral (UV-Vis/DRS) studies were carried out on a Perkin-Elmer lambda-650 DRS UV-Visible spectrophotometer. The EPR spectra of copper(II) complexes were recorded at LNT on a Varian E-4 X-band spectrometer using TCNE as the g-marker (2.0023). The XPS analysis was carried out on a XM1000 Omicron nanotechnology XPS system using Al-Kα monochromatic radiation. The samples were made in to pellets and were used as such for X-ray Photoelectron Spectroscopic (XPS) studies. The crystalline nature of the materials were ascertained by powder X-ray diffraction pattern using Bruker D8 advance diffractometer with monochromatic Cu-$K\alpha_1$ radiation (λ=1.5418 A°). TGA experiments were performed with Versa Therm Cahn Thermo balance TG-151 with a sensitivity of 10μg. TGA experiments were conducted in the temperature range of 300-1150 K with 20 ± 0.01 mg of the samples and the analyses were carried out at a heating rate of 10 K/min under static air atmosphere. The N_2 adsorption, desorption isotherms and Brunauer-Emmett-Teller (BET) surface area measurements at 77 K were carried out on a Micrometrics ASAP (Model 2020) surface area analyzer with nitrogen and helium gases with a purity of 99.999%. HRTEM analysis was carried out on a FEI TECNAI G2 (T-30) transmission electron microscope with an accelerating voltage of 250 KV.

Synthesis of O,O'-mono methylene bis(salicylidene) (SL)

Salicylaldehyde (0.61 g, 5 mmol) was dissolved in 20 mL of DMF to which potassium carbonate (1.73 g, 12.5 mmol) was added and the mixture was stirred at room temperature. To this mixture 1,1 diidomethane (0.6 g, 2.5 mmol) was added and then stirred under reflux for 6 h. The resulting mixture was partitioned between water and ethylacetate. The ethyl acetate layer was collected, concentrated under reduced pressure and was then subjected to silica gel (100-200 mesh) column chromatography using hexane-ethylacetate (1:9) as eluent to afford the product (1.1g ; 90%) in pure form. The purified SL was characterized by spectral studies and the results were compared with those of earlier reports.[20] ^{1}H NMR ($CDCl_3$, 400 MHz): δ: 2.4 (2H, p, CH_2O), 4.33 (4H, t, J = 7.6 Hz, OCH_2O), 7.03 (4H, m, Ar-H), 7.55 (2H, t, J = 7.7 Hz, Ar-H), 7.83 (2H, d, J = 7.7 Hz, Ar-H), 10.49 (2H, s, aldehyde-H); ^{13}C NMR ($CDCl_3$, 100 MHz):ppm: 29.2, 64.7, 112.5, 121.0, 124.9, 128.8, 136.2, 161.0, 189.6.

Synthesis of Schiff base ligand with 3-APTES (SLTES)

The O,O'-mono methylene bis(salicylidene) (SL) (0.5g, 2mmol) was dissolved in 50 mL of ethanol and to this 3-APTES (1 ml, 4.2 mmol) was added. The solution was refluxed for 6 h and the resulting dirty white solid was washed with hot ethanol, acetone and diethyl ether, dried under vacuum for 6 h. Yield: 1 g (80%).

Synthesis of MCM-41 by sol-gel process

The siliceous mesoporous silica was synthesized according to the reported procedure.[21] The typical synthesis involves dissolving 2 g of CTAB in 120 mL of deionised water containing 1 g of NaOH by heating at 323 K. To this solution 6 mL of TEOS was added and the mixture was vigorously stirred at room temperature for 6 h and aged at 383 K for 24 h in an autoclave under static air condition. The product was isolated by filtration and washed with deionised water and methanol. The resulting white powder (SLTES) was dried at 383 K overnight and calicined at 800 K for12 h, Yield: 0.3 g.

Grafting of Schiff base ligand with Si-MCM41 (SiOF)

About 0.1 g of the Si-MCM41 was suspended in 30 mL toluene along with 0.2 g SLTES, and then sonicated for 15 min. The reaction mixture was then heated for 8 h at 363 K.The resulting dirty white solid was washed with ethanol, toluene and dried for 12 h at 373 K. Yield 0.25 g.

Synthesis of solid supported Schiff base complexes (NiOF&CuOF))

0.5mmol of M(II)[M(II):Ni(II)&Cu(II)] chloride salts were added to an ethanolic solution of 100 mg of SiOF and was refluxed for 3 h and the resulting solids were dried, and Soxhlet extracted with ethanol for 6 h and dried again at 393 K.

Photocatalytic degradation of MO under UV light

The photocatalytic oxidation reactions were carried out in a glass reactor with a diameter of 66 X 98 mm that contains a water jacket at room temperature. A mercury (Hg) lamp (100 W, 365 nm) was used as a UV light source to trigger photo decomposition reactions. The catalyst 0.05 g of SiOF/ 0.05 g of NiOF/ 0.05 g of CuOF and 0.01 mmol of 100 mL aqueous MO dye solution was added to the catalysts separately. The reaction conditions were optimized in dark at room temperature and irradiated under UV light (< 360 nm). The removal percentage and consequent spectral changes at predetermined time intervals were monitored by the UV-Visible absorption

spectra at 464 (± 1) nm for 4.5 h. The percentage conversion was determined by the following equation.

% Conversion = $(A_0-A_t)/A_0*100$ (1)

where A_0= Initial absorbance, A_t = Absorbance at time (t).

Photocatalytic degradation of RR under UV light

The photocatalytic oxidation reactions were carried out in a glass reactor with a diameter of 66 X 98 mm that contains a water jacket at room temperature. A mercury (Hg) lamp (100 W, 365 nm) was used as a UV light source to trigger photo decomposition reactions. The catalyst 0.05 g of SiOF/ 0.05 g of NiOF/ 0.05 g of CuOF and 0.01 mmol of 100 mL aqueous RR dye solution was added to the catalysts separately. The reaction conditions were optimized in dark at room temperature and irradiated under UV light (< 360 nm). The removal percentage and consequent spectral changes at predetermined time intervals were monitored by the UV-Visible absorption spectra at 519 (± 1) nm for 7 h. The percentage conversion is calculated from equation (1)

Results and discussion

Fourier Transform IR Spectroscopy

The FTIR spectra of the SL, SLTES, SiOF, NiOF and CuOF are provided in **Fig. S3 (ESI†).** The shift in band positions and their peak assignments in wave number are listed in **Table 1.** The disappearance of SL aldehyde carbonyl group at 1720 cm^{-1} and the formation of a new peak at 1642 cm^{-1} due to azomethine (-C=N) group in the Schiff base ligand *i.e* SLTES were observed.[22, 23] The SLTES shows bands at 2805, 2918, 3012, and 3185 cm^{-1}, for the aliphatic and aromatic C-H vibrations and a peak at 1600 cm^{-1} is attributed to the C=C phenyl ring stretching frequencies. SLTES shows typical absorption bands in the region of 2970-2850 cm^{-1} associated with the -CH_2 group vibrations of the SL ligand,[24] which clearly indicates that the primary amino group of the APTES was involved in the formation of the azomethine with SL. The FTIR spectrum of the SiOF indicates that a change in the coordination sphere of the ligand has taken place. In this context, the new broad bands around 1080 cm^{-1} may be attributed to the formation of Si-O-Si linkages with appended SLTES.[25]

The SiOF also shows peaks at 2968 cm^{-1} due to the aliphatic and aromatic C-H vibrations. The N=C group frequency is observed at 1642 cm^{-1} for SLTES, but in the case of

NiOF and CuOF this peak appears at 1615-1632 cm^{-1} due to metal ion coordination with nitrogen atoms. At lower frequency region, the complexes exhibit medium intensity bands in the region of 420-450 cm^{-1} and 520-600 cm^{-1}, corresponding to M-N and M-O vibrations, respectively,[26] indicating that M(II) ion coordinates with two aromatic ether oxygen atom and two azomethine nitrogens. The broad shoulder at 1630-1640 cm^{-1} is due to the bending frequency of the O-H group present on the surface and the azomethine (-N=C) group vibrations may combine in this region.The structure of Si-MCM41 silica frame work has not changed during anchoring. The FTIR spectral data provide evidence for the anchoring of Schiff base metal complexes and their stability in the pores of Si-MCM41.

Table 1: FTIR spectral frequencies (cm^{-1})of the free and encapsulated complexes.

Sample	Wave number (cm^{-1})							
	$\nu_{(C=O)}$	$\nu_{(C=N)}$	$\nu_{(C–O–C)}$	$\nu_{(Si-O)}$	$\nu_{(C-C)}$	$\nu_{(C=C)}$	$\nu_{(M–O)}$	$\nu_{(M–N)}$
SL	1706	-	1253, 1321	-	1525	1601	-	-
SLTES	-	1638	1221, 1302	1085	1560	1599	-	-
MCM41	-	-	-	1086	-	-	-	-
SiOF	-	1645	1248, 1306	1086	1563	1606	-	-
NiOF	-	1613	1244, 1305	1083	1542	1574	556	425
CuOF	-	1620	1245, 1310	1090	1565	1542	578	441

Diffuse Reflectance Spectra

The DRS UV-Visible spectra of the NiOF and CuOF were recorded in the range of 200-800 nm and the spectral traces are provided in Fig.1.The NiOF shows two characteristic bands at 278 and 339 nm due to $\pi \rightarrow \pi^*$ and $n \rightarrow \pi^*$ transitions respectively and a broad band centred at 630 nm due to d-d transition. The $n \rightarrow \pi^*$ transition at 278 nm is assignable to the phenyl rings, whereas the bands in the region of 390–410 nm are assignable to the $n \rightarrow \pi^*$ transition of the (C=N) moiety. CuOF also shows the corresponding peak values at 285 nm and 316 nm, which

are assigned to π→π* and n→π* transitions respectively.[27] The bands due to d-d transition of similar energies correspond to the $T_{2g} \rightarrow E_{2g}$ transition of the Ni(II) centres. The CuOF shows a broad peak at 622 nm due to d-d transition. The NiOF and CuOF samples exhibit several high intensity CT and intra-ligand bands in the range of 260-430 nm. The CT and d-d transitions afforded evidences for the complexation of Ni(II) and Cu(II) ions with the Schiff-base ligand. The electronic spectra of Cu(II) complexes show two bands near 630 nm (broad) and 400 nm (shoulder), attributed to $^2B_{1g} \rightarrow {}^2A_{1g}$, $^2B_{1g} \rightarrow {}^2B_{2g}$ and $^2B_{1g} \rightarrow {}^2E_g$ transitions.[28] This is due to the ligand to metal charge transfer (LMCT) bands in addition to the π→π* of phenolic and imine-N which is coordinated to M(II).

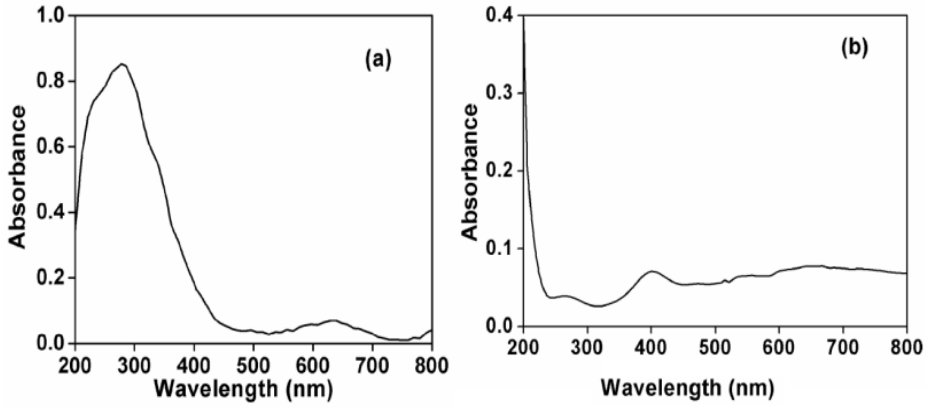

Fig. 1: DRS UV-Visible spectra of (a) NiOF and (b) CuOF

EPR spectral studies

The EPR spectrum of CuOF is anisotropic and the nitrogen hyperfine splitting can be clearly seen in the spectrum(Fig.2) The Cu(II)L.2ClO_4 shows values of $g_{\|}$, $g_{\perp}$ and g_{av} at 2.24, 2.082 and 2.13 respectively. The $g_{\|} > g_{\perp} > 2.0023$ indicates the covalent environment of the metal ion with the Schiff base and also the hyper fine splitting factor ($A_{\|}$) value at 109.5 G. [27,29]

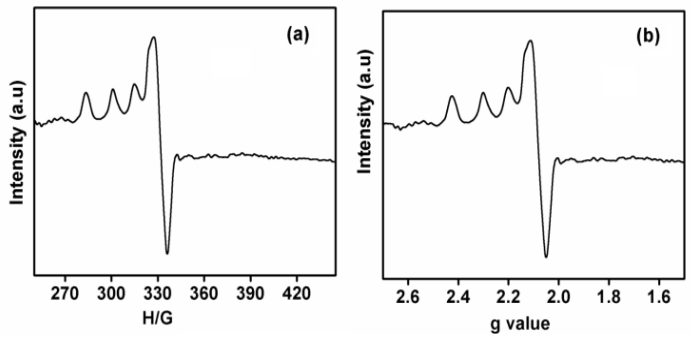

Fig.2: EPR spectrum of the supported complex CuOF

Powder X-ray diffraction

The power XRD studies of the calicined MCM41, SiOF, NiOF and CuOF were recorded at room temperature(Fig.3). The XRD pattern of the parent MCM41 sample shows three low-angle strong reflections at d_{100}, d_{110} and d_{200} planes and a weak one at d_{210} plane. This is characteristic of hexagonal Si-MCM41 structure with a d_{100} spacing value of 40.83 A°. The SiOF also shows the same characteristic feature as Si-MCM41 with d_{100} spacing value of 42.1 A°. The relative peak intensity values of (1 0 0), (1 1 0) and (2 0 0) reflections for NiOF and CuOF decrease when compared to that of Si-MCM41and d_{210} plane was not observed. The unit-cell parameters calculated using d_{100} were (d_{100} = 43.3 A°, 2θ = 2.21°) and (d_{100} = 43.95 A°, 2θ = 2.28°) for NiOF and CuOF respectively.[30,31] The XRD pattern of NiOF and CuOF with decreased peak intensity and a change in d_{100} spacing value suggests the presence of Schiff base complex in the silica matrices. This is attributed to the lowering of the local order, such as wall thickness or it might be due to the reduction of the scattering contrast between the porous silica channel and the Schiff base moiety. However, XRD parameters show that the crystalline nature of Si-MCM41 has not changed during the grafting process.

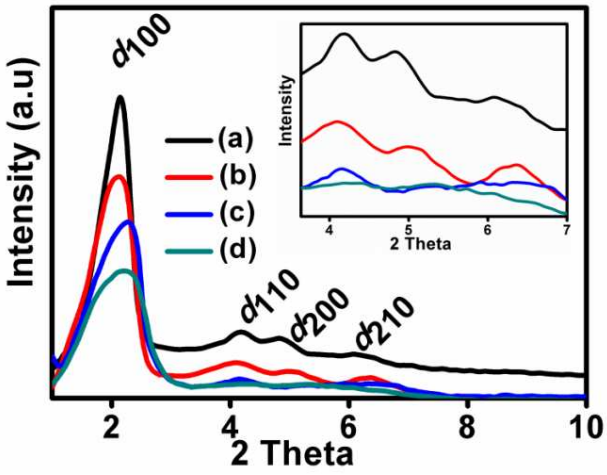

Fig.3: Power XRD pattern of (a) MCM41 (b) SiOF (c) NiOF and (d) CuOF (inset diagram shows expanded spectra between 2θ =3.5° to 7°)

X-ray photoelectron spectroscopy

X-ray photoelectron spectroscopy (XPS) is a powerful technique which is used to investigate the electronic properties of the species formed on the surface. XPS studies reveal the electronic environment, *i.e.,* oxidation state and spin multiplicity, which influence the binding energy of the metal electronic transitions. Fig.4 reveals the presence of C, N, O, Si, Ni(II) and Cu(II), which confirms the respective oxidation state of the elements. These peaks are related to carbon in the encapsulated complexes which show medium intensity broad bands. The C1s, N1s and O1s and Si2p appear at 285.1, 400.0, 531.2 and 103.2 eV respectively.[32] The XPS traces of NiOF indicate that no shake-up satellite peaks are observed below 876 eV for Ni(II)(2p) which confirms the planar form and diamagnetic nature of Ni(II) (Fig.4c). NiOF exhibits XPS traces at the binding energy values of 854.13 eV and 874.61 eV for $2p_{3/2}$ and $2p_{1/2}$ states respectively.[33] Fig.4d shows that the compound CuOF has shakeup satellite suggesting that copper is in +2 oxidation state. The Cu 2p level XPS traces of the CuOF indicate the paramagnetic nature of the Cu(II) ion. These observations confirm the presence of an unpaired electron in $dx^2–y^2$ orbital, and the EPR spectral data also support the same . CuOF exhibits the XPS traces with the binding energy values of 934.10 eV and 954.91 eV for $2p_{3/2}$ and $2p_{1/2}$ states respectively.[34-36.]

Table 2: Binding energy of the NiOF and CuOF (M(II):Ni&Cu)

Sample	Binding energy (eV)				
	Si(2p)	C(1s)	O(1s)	N(1s)	M(II) (2p)
NiOF	102.5	284.3	532.0	400.1	854.3, 874.6
CuOF	102.6	284.2	532.4	400.8	934.9, 954.3

Fig. 4: XPS survey spectra of (a) NiOF, (b) CuOF; (c) Ni(II) 2p and (d) Cu(II)2p core level spectra.

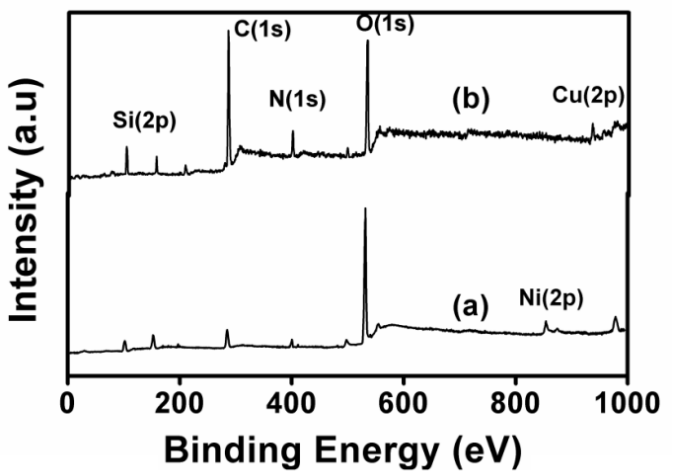

Surface area analysis

The BET surface area, N_2 adsorption/desorption isotherms and pore volume of the materials Si-MCM41, SiOF, NiOF and CuOF are shown in Fig.5. The pore size distribution curves of the samples were evaluated from the sorption branches of the isotherms using Barrett-Joyner-Halenda method and the encapsulated complexes show type-IV isotherm. At relatively low pressures ($P/P0 \leq 0.3$), the N_2 adsorption isotherm of the NiOF and CuOF was different from that of MCM41 due to N_2 uptake. A steep increase observed after P/P_0 at 0.4 reflects their narrow pore size distribution due to capillary condensation in the pores by the Schiff base ligand and its metal complexes. The surface area of Si-MCM41 was found to be 900 m^2/g. However, in the case of SiOF, NiOF and CuOF the surface area is drastically reduced to 580 m^2/g, 310 m^2/g and 350m^2/g, respectively. The average pore width of Si-MCM41 is 3.8 nm and it is reduced to 3.2 nm, 0.8 nm and 1.3 nm, for SiOF, NiOF and CuOF respectively. The average pore volumes are 0.54 cm^3/g, 0.35 $cm^3/$ g, 0.18 $cm^3/$ g, and 0.23 $cm^3/$ g for Si-MCM41, SiOF, NiOF and CuOF respectively. The pore volumes get drastically reduced during grafting and it can be attributed to the increased loading with organics, which occupy void space inside the

mesopores.[37,38] This analysis confirms that NiOF and CuOF have same structural integrity even during the anchoring process.

Thermal analysis (TGA)

The TG/DTG curves of the MCM41, SiOF, NiOF and CuOF were recorded in the static air atmosphere and are shown in Fig.6. The DTG curves show a residual mass of around 64%, clearly suggesting the thermal stability of all the composites. The DTG curves of the materials show multi step decomposition. The composites show a mass loss around 6% in the first stage up to 530 K, due to the water molecules present on the surface. In case of the SiOF, the decomposition during the first step between 343 K and 530 K corresponds to the loss of coordinated water molecules with the mass loss of 5.7%. In the second step up to 790 K, there is a continuous mass loss of 12.5 % by SL moiety in Schiff base complexes with a residual mass around 81.5%. The NiOF and CuOF systems show higher thermal stability with a residual mass around 63%. The second and the third stage of mass loss around 30% up to 953 K are due to the loss of Schiff base complexes and the formation of metal oxide residues.[39]

TEM analysis

The TEM photograph of the parent MCM41, NiOF and CuOF are shown in Fig.7. The solid support has hexagonal shape and its channels are well ordered. The NiOF and CuOF systems also exhibit hexagonal geometry and are well ordered with slight change in the morphology and negligible agglomeration when compared to that of the parent mesoporous silica.[40,41]

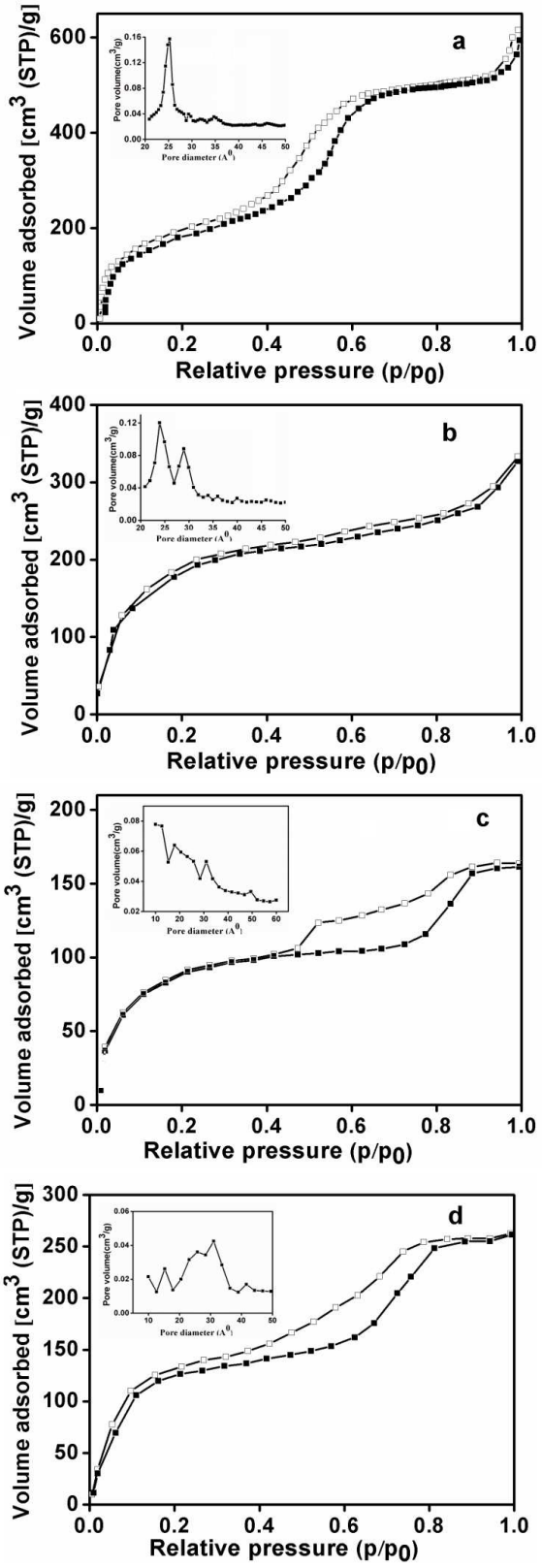

Fig. 5: N_2 adsorption-desorption isotherms (a) Si-MCM41 (b) SiOF (c) NiOF and (d) CuOF.

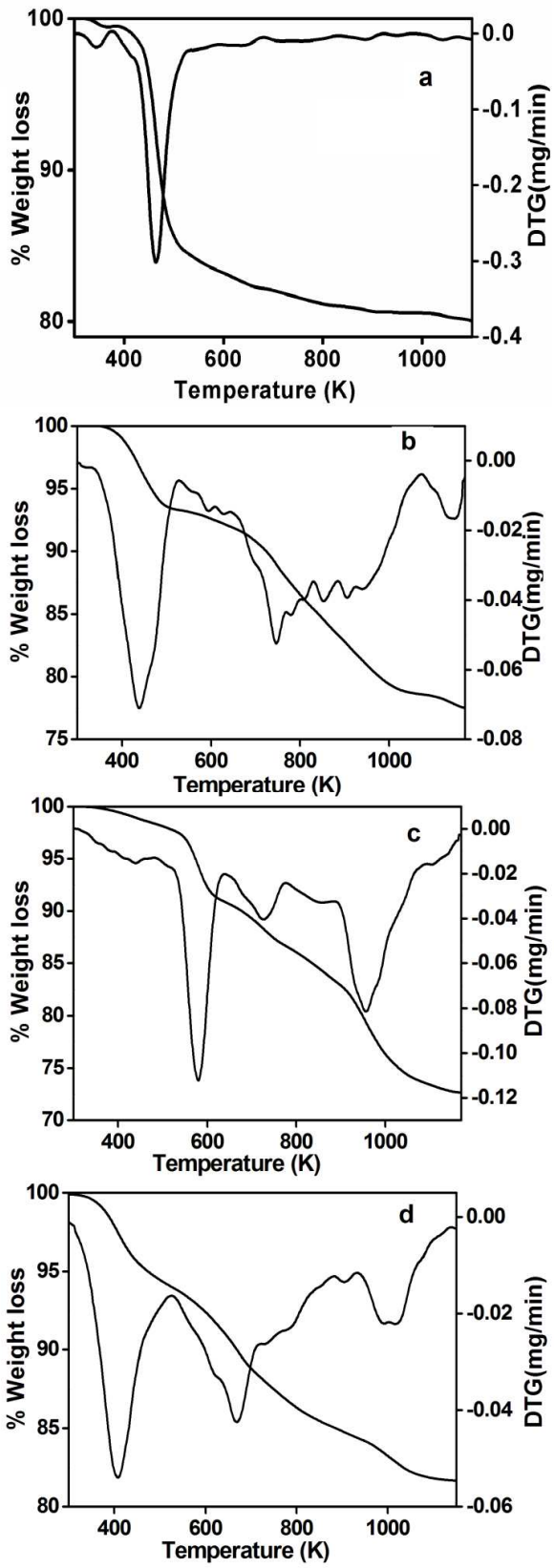

Fig.6: TG /DTG curves of (a) Si-MCM41(b) SiOF (c) NiOF and (d) CuOF

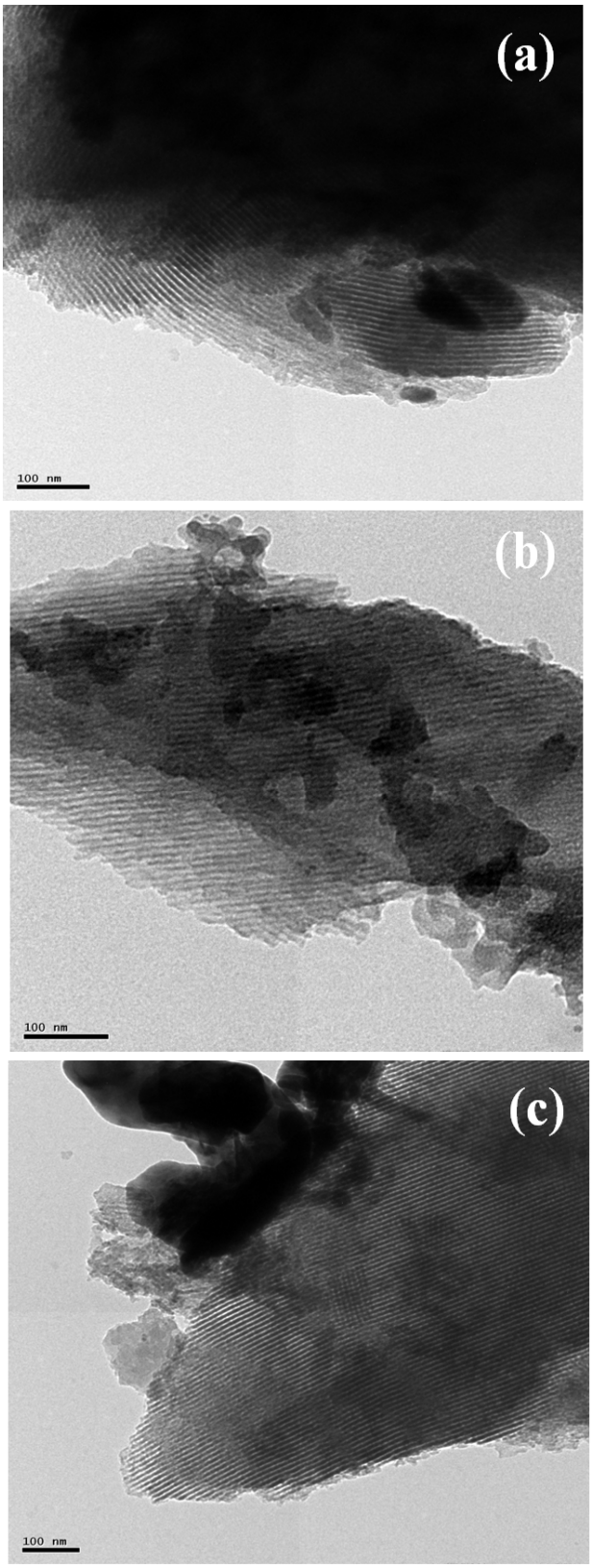

Fig.7: TEM images of (a) Si-MCM41 (b) NiOF and (c) CuOF

Catalytic studies

Mechanistic issues involved in photocatalysis

The photo degradation of MO in the presence of MCM41, SiOF, NiOF and CuOF, under UV light irradiation has been investigated. The efficiency of the catalyst in methyl orange degradation was calculated from the optical absorption spectral analysis. The aliquot samples of the reaction medium were collected and the consequent absorption changes were recorded at 464 (± 1) nm.[42] The spectral changes in the dye degradation by (a) Si-MCM41 (b) SiOF (c) NiOF and (d) CuOF are given in Fig S4 (ESI†). The MOF exhibits higher degradation efficiency, when compared to that of SiMCM and SiOF. The removal percentages are 20%, 12%, 83% and 100% for Si-MCM41, SiOF, NiOF and CuOF respectively (Fig.8a). The efficiency of the catalyst in the degradation of RR was calculated by the optical absorption spectral analysis. The aliquot samples of the reaction medium were collected and the consequent absorption changes were recorded at 520 (± 1) nm and are given in Fig.S5 (ESI†).[43] The removal percentages are 18%, 27%, 87% and 100% for Si-MCM41, SiOF, NiOF and CuOF respectively (Fig.8b).

Metal complex enhances the acidity of the composites during grafting process. The photocatalytic performance and the removal efficiency of the reactive red increases. MOF can decrease the recombination of electron-hole pair and increase the photocatalytic performance.[44] The MOF shows higher activity because of its metal loading efficiency which enhances the photo generated electron pairs (e^- and h^+). Photogenerated-holes and electrons may react with the surface hydroxyl groups to generate active oxidative ionic radical ($O_2^{\bullet-}$ and $^{\bullet}OH$) from the reaction medium. The photo generated electrons exhibit more efficiency towards the hole formation and minimize the band gap energy, meanwhile, the formation of $^{\bullet}OH$, $^{+\bullet}O_2H$, $^{-}O_2$ radicals, which are powerful oxidants, starts a cascade of oxidation reactions that can convert the organic compounds in solution completely into NO_2^-, NO_3^- , SO_4^{2-} ions H_2O and CO_2 in reactive red 198 (SO_4^{2-} ions, H_2O, CO_2 in the case of MO) and other inorganic compounds.[45-47] After the completion of the reaction, NiOF and CuOF were recovered and their catalytic efficiency was tested in five cycles and overall percentage is provided in Fig. S6 (ESI†).

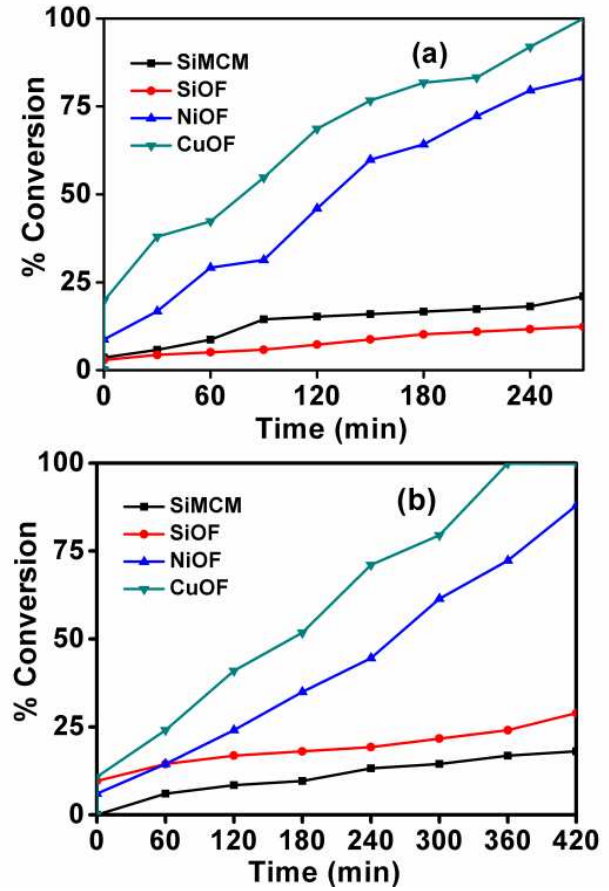

Fig. 8: The percentage degradation of MO (a) and RR (b) by Si-MCM41 (b) SiOF (c) NiOF and (d) CuOF.

Summary

The nickel(II) and copper(II) complexes of the Schiff base ligand O, O'- mono methylene bis(salicylidene aptes) were synthesized by the condensation with 3-aminopropyl triethoxysilane (3-APTES) which was subsequently grafted with silica. The covalently anchored metal complexes were investigated by several spectral, thermal, sorption and microscopic techniques. The solid state catalysts were employed as photocatalysts in the degradation of MO and RR under UV irradiation. The CuOF showed higher activity than that of NiOF in the dye degradation reactions. The catalytic activities of the recovered and purified photocatalysts were compared with that of fresh catalysts

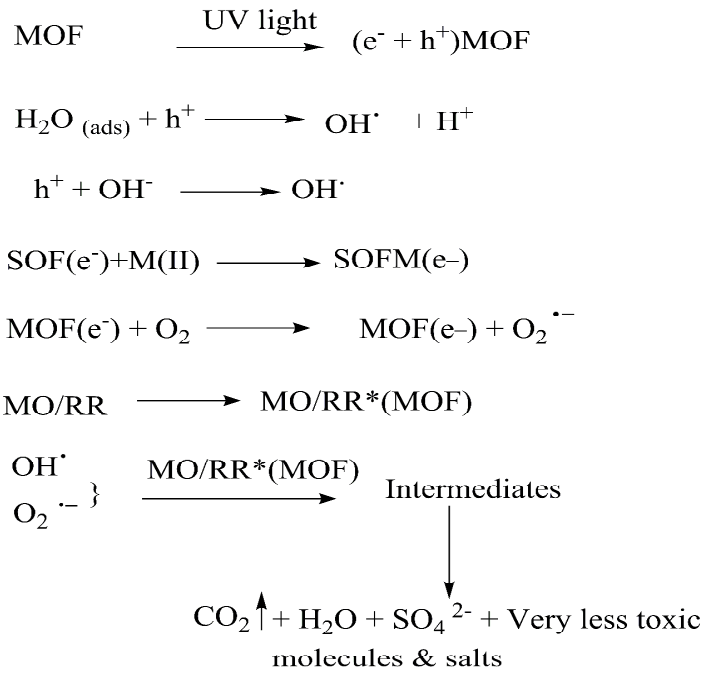

Fig.9: The proposed radical-ion mechanism for the MO and RR dye degradation.

Acknowledgements

The authors are thankful to National Center for Nanoscience and Nanotechnology, University of Madras, Chennai for XPS, DRS and TEM analysis. One of the authors G.Ramanjaneya Reddy is grateful to Dr. G. Bhaskar Raju, Chief scientist, CSIR-NML Madras Complex, Chennai, India for his support during the experimental work.

Appendix A. Supplementary data

The NMR, FTIR, absorption plots of the both degradation reactions, overall percentage conversion of reused catalysts, FTIR and XRD of the recovered MOF are given in the electronic supplementary information.

References

1 S. E. Mourabit, M. Guillot, G. Toquer, J. Cambedouzou, F. Goettmann and A.Grandjean, *RSC Adv.,* 2012, **2**, 10916.

2 T. F. Parangi, R. M. Patel and U. V. Chudasama, *Bull. Mater. Sci*., 2014, **37**, 609.

3 S. Gulati, A. Pandey and A. Adholeya, *Appl. Catal. B: Env*. 2012, **125**, 247.

4 M. Kruk, M. Jaroniec and A. Sayari, *Microporous Mesoporous Mater*., 2000, **35–36,** 545..

5 A. Modak, J. Mondal, V.K. Aswal and A. Bhaumik, *J. Mater. Chem.,* 2010, **20**, 8099.

6 S. Li, J.Zheng,D. Chen, Y.Wu, W. Zhang, F. Zheng, J.Cao, H. Ma and Yaling Liu , *Nanoscale,* 2013, **5**, 11718

7 W. Zhang, J. Zheng, C. Tan, X. Lin, S. Hu, J. Chen, X. You and S. Li, *J. Mater. Chem. B.*, 2015, **3**, 217.

8 M. Li, L. Liu, L. Zhang, X. Lv, J. Ding, H.Hou and Y. Fan, *Cryst. Eng. Comm.*, 2014, **16**, 6408.

9 D. Chatterjee, E. Ember, U. Pal, S. Ghosh and R. V. Eldik, *Dalton Trans.,* 2011, **40**, 10473.

10 R. B. N. Baig and R. S. Varma, *Chem. Commun.,* 2013, **49,** 752.

11 A. Corma and H. Garcia, *Chem. Rev*., 2002, **102,** 3837.

12 K. Chennakesavulu, M. M. Reddy, G. R. Reddy, A. M. Rabel, J. Brijitta, V. Vinita, T. Sasipraba, J. Sreeramulu, *J. Mole. Struct,* 2015, **1091**, 49.

13 P. Niu and J. Hao, *Colloids Surf. A*, 2014, **443**, 501.

14 S. C. Kim, B. Y. Jeong, and D. K. Lee, *Top Catal*, 2005, **33**, 1.

15 Priyanka and V. C. Srivastava, *Ind. Eng. Chem. Res*., 2013, **52**, 17790.

16 W. Li, D. Li, J. Wang, Y. Shao, J. You and F. Teng, *J. Mol. Catal. A: Chem.*, 2013, **380,** 10.

17 M. A. Tabarra, H. A. Mallah and M. M. E. Jamal, *J. Chem. Technol. Metall.*, 2014, **49**, 247.

18 O. Merka, V. Yarovyi, D. W. Bahnemann and M. Wark, *J. Phys. Chem. C*., 2011, **115,** 8014.

19 C. Gol, M. Malkoc, S. Yeşilot and M. Durmus, *Dalton Trans*., 2014, **43,** 7561.

20 C. N. Reddy, K. Suman, K. P. Sai, S. Thennarasu and A. B. Mandal, *Dyes Pigments*., 2012, **95,** 606.

21 J. S. Beck, J. C. Vartuli, G. J. Kennedy, C. T. Kresge, W. J. Roth and S. E. Schramm, *Chem. Mater.,* 1994, **9,** 1816.

22 S. Bhunia and S. Koner, *Polyhedron,* 2011, **30,** 1857.

23 S. M. Islam, N. Salam, P.Mondal and A. S. Roy, *J. Mol. Catal. A: Chem.*, 2013, **366**, 321.

24 V. Z. Mota, G. S. G. Carvalho, P. P. Corbi, F. R. G. Bergamini, A. L. B. Formiga, R. Diniz, M. C. R. Freitas, A. D. Silva and A. Cuin, *Spectrochim. Acta Part: A.*, 2012, **99,** 110.

25 I. C. Chisem, J. Rafelt, J. Chisem, J. H. Clark, D. Macquarrie, M. T. Shieh, R. Jachuck, C. Ramshaw and K. Scott, *Chem. Commun.*, 1998, **18,** 1949.

26 E. Mezui, E. Delahaye, G. Rogez, and P. Rabu, Eur. *J. Inorg. Chem.*, 2012, **32,** 5225.

27 A. R. Silva, K. Wilson, A. C. Whitwood, J. H. Clark, and C. Freire, Eur. *J. Inorg. Chem.*, 2006, 1275.

28 Y. M. Liu, W. L. Feng, T. C. Li, H. Y. He, W. L. Dai, W. Huang, Y. Cao and K. N. Fan, *J. Catal.,* 2006, **239,** 125.

29 M. Zamadics and L. Kevan, *J. Phys. Chem.*, 1993, **97,** 10102.

30 S. G. Renaudin, F. Gaslain, C. Marichal, B. Lebeau, R. Schneider and A. Walcarius. *New J. Chem.,* 2009, **33,** 528.

31 S. Suvanto, J. Hukkamaki, T. T. Pakkanen and T. A. Pakkanen, *Langmuir,* 2000, **16,** 4109.

32 J. Wei, D. B. Ravn, L. Gram and P. Kingshott, *Colloids Surf. B.*, 2003, **32,** 275.

33 M. S. Niasari and M. Bazarganipour, *Appl. Surf. Sci.,* 2008, **255**, 2963.

34 J. L. Cao, L.T. Li and Z. L. Gui, *J. Mater. Chem.,* 2001, **11,** 1198.

35 K. Zhang, K. F. Lam, B. Albela, T. Xue, L. Khrouz, Q.W.Hou, E. H. Yuan, M. Y. He and L. Bonneviot, *Chem. Eur. J.*, 2011, **17**, 14258.

36 O. Franke, J. Rathousky, G. S. Ekloff and A. Zukal, *Stud. Surf. Sci. Catal.*, 1995, **91** 309.

37 P. Sharma, J. K. Seong, Y. H. Jung, S. H. Choi, S. D. Park, Y. Yoon and H. Baek*, Powder Technol.*, 2012, **219**, 86.

38 S. L. Jain, B. S. Rana, B. Singh, A. K. Sinha, A. Bhaumi, M. Nandi and B. Sain, *Green Chem.*, 2010, **12**, 374.

39 C. W. Kwong, C. Y. H. Chao, K. S. Hui and M. P. Wan, *Environ. Sci. Technol.*, 2008, **42** 8504.

40 R. Nejat, A. R. Mahjoub, Z. Hekmatian and T. Azadbakht, *RSC Adv.*, 2015, 5, 16029.

41 S. Yamazaki and N. Nakamura, *J. Photochem. Photobiol: A.*, 2008, **193**, 65.

42 Y. Fu, H. Chen, X. Sun and X. Wang, *Appl. Catal: B,*, 2012, **111-112**, 280.

43 G. Moussavi and R. Khosravi, *Bioresource Technol.*, 2012, **119**, 66.

44 G. R. Reddy, S. Balasubramanian and K. Chennakesavulu, *J. Mater. Chem. A*, 2014, **2,** 15598.

45 S. Kuriakose, B. Satpati and S. Mohapatra, *Phys. Chem. Chem. Phys.*, 2014, **16**, 12741.

46 L. Yu, J. Xi, M. Li, H. Chan, T. Su, D. Phillips and W. Chan, *Phys. Chem. Chem. Phys.*, 2012, **14**, 3589.

47 L. Wen, J. Zhao, K. Lv, Y. Wu, K. Deng, X. Leng and D. Li, *Cryst. Growth Des.,* 2012, **12,** 1603.

Synthesis, characterization and photocatalytic studies of mesoporous silica grafted Ni(II) and Cu(II) complexes

G. Ramanjaneya Reddy,[a] and S. Balasubramanian[a]*

[a]Department of Inorganic Chemistry, School of Chemical Sciences, University of Madras, Guindy Campus, Chennai-600 025, India.
E-mail:bala2010@yahoo.com; Tel: +91 9444016707, 044 22202794, Fax: +91 4422300488

Graphical abstract